Effect of Liquid−Liquid Phase Separation on the Lamellar Crystal Morphology in PEH/PEB Blend

Xiaohua Zhang,[†,⊥] Zhigang Wang,[‡] Ruoyu Zhang,[†,§] and Charles C. Han*[,†]

Beijing National Laboratory for Molecular Sciences, Joint Laboratory of Polymer Science and Materials, State Key Laboratory of Polymer Physics and Chemistry, CAS Key Laboratory of Engineering Plastics, Institute of Chemistry, Chinese Academy of Sciences, Beijing 100080, China, and Graduate School of the Chinese Academy of Sciences

Received August 8, 2006; Revised Manuscript Received November 3, 2006

ABSTRACT: Optical microscopy (OM) and atomic force microscopy (AFM) were used to investigate the effect of liquid−liquid phase separation (LLPS) on the lamellar crystal morphology in a statistical copolymer blend of poly(ethylene-*co*-hexene) (PEH) and poly(ethylene-*co*-butene) (PEB). The quench depth and the time of liquid−liquid phase separation (LLPS) exhibit obvious influences on the lamellar crystal morphology. The values of lamellar long period were measured from the AFM micrographs. It is interesting to find that the lamellar long periods of the blend show minimum values with respect to the LLPS temperature, LLPS time, and the crystallization temperature. The lamellar insertion and lamellar thickening models and inclusion/exclusion of the amorphous component in the lamellar stacks are considered to cause this puzzling phenomenon.

Introduction

In recent years, the statistical copolymer blends of polyolefins have received a lot of attention. The requirement to enhance the material properties and the desire to have a better understanding of the underlying mechanism for the formation of various structures and morphologies have triggered this type of research. In particular, there have been significant fundamental and industrial technological interests in polyolefin blends. Although critical phenomena and phase separation in binary mixtures have been well studied and reasonably understood,[1−4] the complexity of the interplay between liquid−liquid phase separation (LLPS) and another phase transitions such as crystallization remains largely unexplored.[5] In recent studies by Wang et al., the nearly isorefractive polyolefin blends consisting of two branched metallocene polyethylenes were investigated,[6−8] and the phase diagram of LLPS was constructed (Figure 1).[4] The authors used indirect evidence provided by a range of techniques, including diffuse light scattering, to identify the phase boundaries. The studies revealed the existence of an upper critical solution temperature (UCST) as well as the composition dependence of the LLPS boundary, which followed the prediction of Flory−Huggins mean-field theory for the binary polymer mixtures. Because of the microstructural similarity between PEH and PEB components, it is difficult to distinguish the two coexistent phases during phase separation by microscopy and/or scattering technique; however, it is still scientifically important to measure the LLPS. Up to now, most studies have focused on identification of the existence of LLPS through the scattering measurements[9−12] or morphological studies,[12−14] but those focusing on the effects of LLPS on the crystal morphologies have received relatively limited attention. In this study, we used the same blend system that was employed by Wang et al.[4] The crystallization rate vs temperature of neat PEH and the LLPS rates at the temperatures of interest have been investigated.[7,15] We will present our experimental results on this polyolefin blend system in the regions that have not been explored before. This blend system has a UCST immiscible region with $T_c = 146$ °C and the critical composition $\phi_c = 0.44$ in the melt. We will demonstrate an interesting observation that is the average long periods of the lamellar stacks measured in the isothermally annealed samples by AFM reveal the minimum values depending on the quench depths or time of LLPS or the crystallization temperature, T_c. We will further discuss the possible origin of the minimum values of the lamellar long periods.

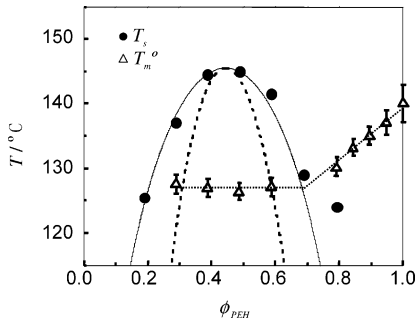

Figure 1. Phase diagram of PEH/PEB blends. The symbols (filled circles) correspond to the experimental data points of binodal temperature (T_s) and the solid line to the fit of the Flory−Huggins theory. The additional symbols (open triangles) display the equilibrium melting points of the indicated blends.

Experimental Section

Materials and Blend Preparation. The materials used in this study were supplied by ExxonMobil Co. Ltd. They are statistical copolymers of ethylene and 1-hexene (PEH) ($M_w = 110$ kg/mol, 2 mol % hexene comonomer) and of ethylene and 1-butene (PEB) ($M_w = 70$ kg/mol, 15 mol % butene comonomer). Since they were synthesized with metallocene catalysts, the samples have relatively narrow polydispersity (∼2). PEH is the only crystallizable component of this blend system above 60 °C. The blend of PEH and PEB, which has PEH mass fraction of 40%, denoted as H40, was prepared by the coprecipitation method. PEH and PEB samples in mass ratio of 40 to 60 were first dissolved in hot xylene at 120 °C,

* To whom correspondence should be addressed: e-mail: c.c.han@iccas.ac.cn; Tel +86-10-82618089, Fax +86-10-62521519.
† State Key Laboratory of Polymer Physics and Chemistry.
‡ CAS Key Laboratory of Engineering Plastics.
§ Graduate School of the Chinese Academy of Sciences.
⊥ Now at National Institute of Standards and Technology, Gaithersburg, MD.

10.1021/ma061801a CCC: $33.50
Published on Web 12/07/2006

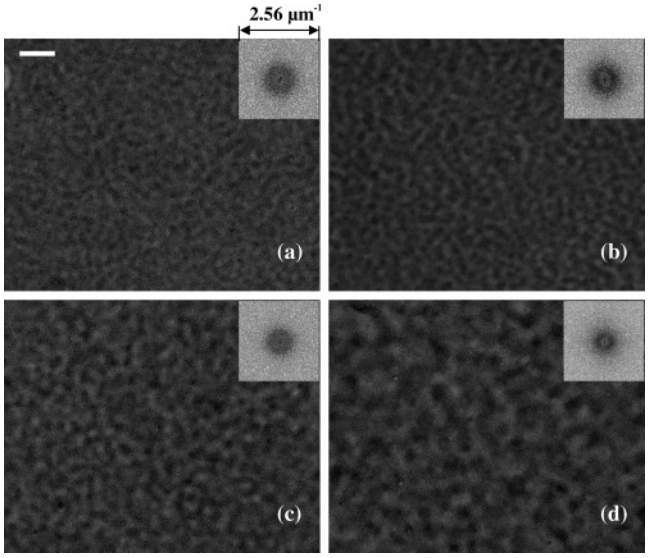

Figure 2. Phase contrast optical micrographs of H40 sample annealed at 135 °C for (a) 4, (b) 6, (c) 10, and (d) 20 h. The scale bar in (a) corresponds to 10 μm and also applies to (b)−(d). The inset shows the FFT image from each micrograph.

and then the solution was cooled to 100 °C and kept for 24 h. Afterward, the solution was poured into chilled methanol to precipitate the blend. After filtration, the obtained blend was washed with methanol and dried in vacuum oven at 30 °C for 72 h. The blend was then hot-pressed at 160 ± 2 °C to form films of 30 μm in thickness and quenched to room temperature for further use.

Characterization by OM and AFM. The phase contrast optical microscopy (PCOM) observations were carried out by using an Olympus (BX51) optical microscope connected to an Olympus (C-5050ZOOM) camera. A Linkam 350 hot stage was used to control the sample temperature.

Tapping-mode AFM observations were performed by using NanoScope III MultiMode AFM (Digital Instruments). Both height and phase images were recorded simultaneously during scanning. The height and phase images were flattened using AFM software to eliminate the height error from the sample. The films of the blend were prepared by a hot press at 160 ± 2 °C between two pieces of silicon wafer with one piece removed after cooling. The film thickness is about 30 μm. The blend melted at 160 °C for 10 min was quenched to the LLPS temperature for annealing and then quenched to the crystallization temperature for isothermal crystallization prior to quenching to room temperature for AFM observation.

Results and Discussion

Figure 2 shows phase contrast optical micrographs of H40 sample melted at 160 °C for 10 min and then isothermally annealed at 135 °C for 4, 6, 10, and 20 h. The 2D fast Fourier transform (FFT) images are shown as insets in Figure 2.

On the basis of the information provided in Figure 1 and ref 4, the H40 sample at 135 °C is within the two-phase region of the phase diagram. Spinodal decomposition mechanism is responsible for the development of bicontinuous, interconnected PEH-rich (dark part)[7,15] and PEB-rich (light part) phases that coarsen with time (Figure 2).

Figure 3 (at large scale) and Figure 4 (at small scale) show atomic force micrographs of H40 sample isothermally crystallized at 117 °C for 64 min after isothermally annealed at 135 °C for different LLPS times. The PEH-rich and PEB-rich domains can be clearly observed after isothermal crystallization at 117 °C for 64 min without experiencing LLPS at 135 °C (Figures 3a and 4a) because of the occurrence of simultaneous liquid−liquid phase separation and crystallization at 117 °C.

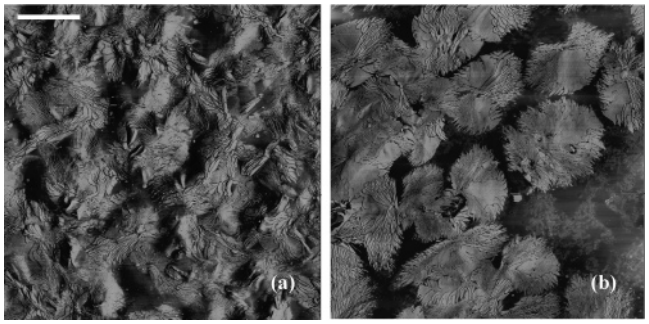

Figure 3. AFM phase micrographs for H40 sample isothermally crystallized at 117 °C for 64 min after isothermally annealed at 135 °C for (a) 0 and (b) 20 h. The scale bar in (a) corresponds to 5 μm and also applies to (b).

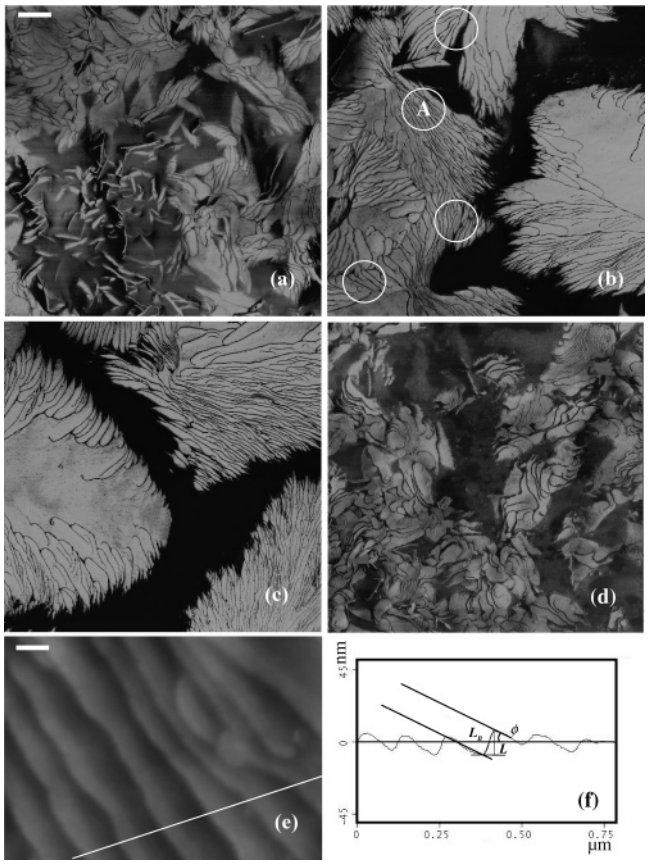

Figure 4. AFM phase micrographs for H40 sample isothermally crystallized at 117 °C for 64 min cooling in the air after isothermally annealed at 135 °C for (a) 0, (b) 6, (c) 20, and (d) 0 h cooling in the liquid nitrogen, (e) height image of the circled part A in (b), and (f) section analysis of (e). The scale bar in (a) is 1 μm and is the same for (b), (c), and (d). The scale bar in (e) is 100 nm.

The following features can be easily found in Figure 4a. Short and small lamellae can be found in the PEB-rich domains. The branched regular lamellar crystals in the spherulites or dendrites are absent. The lamellar crystals in the PEB-rich domains are more imperfect and isolated than those in the PEH-rich domains. Figure 4d shows that under the fast cooling condition (quenched into liquid nitrogen) the short and small lamellae in the PEB-rich domains do not exist any more. Therefore, the lamellar crystals in the PEB-rich domains should form during the cooling to room temperature in air. With the increasing LLPS time, such as after 20 h LLPS, the crystals in the PEB-rich domains cannot be observed (Figure 4c). On the contrary, the lamellae in the PEH-rich domains are larger and more perfect than those in the PEB-rich domains.[16] In particular, the highly branched

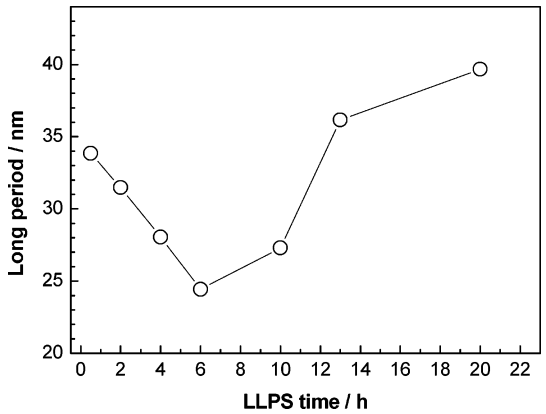

Figure 5. LLPS time dependence of the long period of H40 sample isothermally crystallized at 117 °C for 64 min.

crystal lamellae are formed. The growth proceeds via lamellar fanning out from an initial sheaflike structure, which eventually grows to the hedrite,[8] as is clearly seen in Figures 3b and 4b,c. We can basically explain the above experimental observations as follows. The boundary of two separated domains becomes sharp with the increasing LLPS time. As LLPS becomes more complete, or reaches the "late stages", the two phase-separated phases reach closely the equilibrium coexistent compositions. Thus, the PEB-rich domains cannot give birth to crystals due to the very small amount of remaining PEH component, while the PEH-rich domain can form the large and highly branched lamellar crystals due to the high PEH concentration.

Figure 4 shows that some of the lamellar crystals look like lying flat-on and some lying edge-on. Section analysis of AFM height image shows that the lamellar stacks incline at considerable angles with respect to the image plane. Therefore, for the nonzero inclination angle the local long period of lamellar stacks can be calculated by using eq 1.

$$L_B = \frac{L}{\cos \phi} \tag{1}$$

where L_B denotes the long period, L the vertical distance between the adjacent lamellae measured from AFM height image, and ϕ the angle between the normal to the crystal plane and the image plane. The AFM technique obviously does not offer the possibility to directly measure the tilt angle of the lamellar crystal from the image plane; however, discrimination between the stacks close to flat-on and that inclined at significant angles can still be made from this type of section analysis. With the inclined angle, ϕ, obtained, the lamellar long period can be estimated correspondingly. The averaged long period can be statistically obtained after measuring the local long periods at multiple locations of the different samples with the same annealing conditions in order to get more lamellar stacks. We used the long period for simplicity in the following sections without further emphasis on the statistics of the data unless it is required for the need of discussion.

Figure 5 shows the change of long period of H40 sample isothermally crystallized at 117 °C for 64 min after LLPS at 135 °C for different periods of time. It is seen that the long period decreases at first with LLPS time and reaches a minimum at about 6 h of LLPS, and then the long period starts to increase with the LLPS time. The equilibrium melting points and crystallization temperatures of the blend samples are invariable. It means that the noncrystallizable component, PEB, and phase separation will affect the crystallization and the lamellar thickness. The lamellar microstructure of semicrystalline polymers can contain many stacking defects. In the presence of the defects in the structure, the long period can be affected by the number of lamellae per stack. In this study, the lower PEH concentration on the growth front will form imperfect crystals or baby spherulites, which can be considered as defects existing in the system. Recall that the typical feature of PEH crystals is the strong tendency to form lamellar stacks. Figure 4 shows that the number of lamellae in the stacks increases in addition to the increasing lamellar lateral length from (a) to (b). Besides the progressive formation and growth of the lamellar stacks, the lamellar thickening can happen during crystallization too. Both affect the values of long period. Crystallization mainly proceeds through adding new lamella and/or lamellae between the existing lamellae stacks, thereby increasing the average number of lamellae per stack. The progressive infilling between the initial dilute lamellar stacks by the newly formed lamellae (termed as lamellar insertion model) could lead to a large decrease of long period.[17,18] For polymer blends, inclusion of amorphous component could also cause the increase of long period; in other words, exclusion of amorphous component could cause the decrease of long period. On the basis of our experimental observation, lamellar insertion and lamellar thickening models and inclusion/exclusion of the amorphous component can be brought out together to explain the observed evolution of long period due to the interplay between LLPS and crystallization. The models are schematically shown in Figure 6. Within the short period of LLPS (<6 h), the increasing LLPS time obviously decreases the degree of inclusion of PEB component into the lamellar stacks due to the increasing phase separation. In other words, with the increasing time of LLPS, the crystallizable PEH concentration in the PEH-rich domain increases which gives rise to the increasing number of the lamellae per stack due to the lamellar insertion (Figure 4a,b). The long period thus shows a tendency to decrease with the time of LLPS. When the LLPS time is more than 6 h, the crystallizable PEH concentration in the PEH-rich domains is so high that the PEB component might have the less hindrance on the crystallization of PEH component, provided that we have found that the nucleation rate obviously decreases due to the decreasing in the crossover effect of the spinodal (LLPS) concentration fluctuations at the late stages on the crystallization.[19,20] The lower nucleation rate can give rise to the lower nucleus density compared with the higher nucleation rate case. The total crystallization rate can be separated into the nucleation rate and the growth rate. The linear growth rates of the crystals are the same at the same crystallization temperature and concentration. But the linear crystallization rates of sample undergoing LLPS for different periods of time should be different due to different PEH concentration in PEH-rich domains. The growth rates of the blends with the higher PEH concentration are faster than the lower ones. But the nucleation rate is the slow and "rate controlling" step in most processes. The less hindrance of the noncrystallizable PEB component on

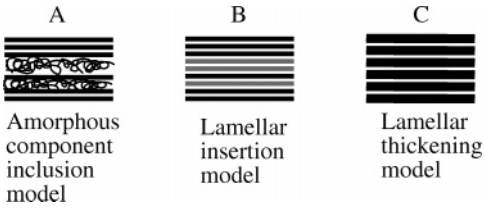

Figure 6. Schematic diagrams of the evolution of the lamellar crystal microstructure, including amorphous component inclusion, lamellar insertion, and lamellar thickening models: (A) increasing long period, (B) decreasing long period, and (C) increasing long period.

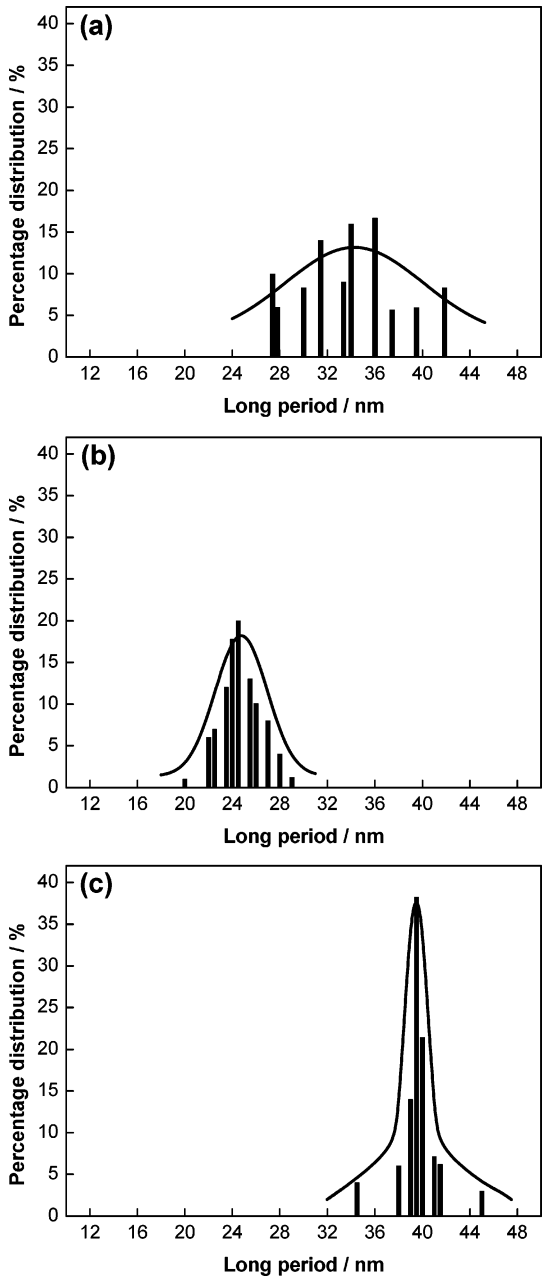

Figure 7. Percentage distribution of long period for H40 sample isothermally crystallized at 117 °C for 64 min after LLPS at 135 °C for (a) 0.5, (b) 6, and (c) 20 h.

the PEH crystal growth fronts and the lower linear crystallization rate can give rise to the thicker lamellae, and accordingly the larger long periods, with narrower statistical distributions. Percentage distributions of the local long periods shown in Figure 7 confirm that for the short LLPS time the long period distribution is wide due to the more rapid crystallization rate which creates stacks with the more and nonuniform amorphous gaps. The linear growth rates of the crystals are the same at the same crystallization temperature and concentration. It means that the lamellar thickness should be the same and the wide distributions of long period are caused by the more and nonuniform amorphous gaps. With the increasing LLPS time, the averaged long period moves to lower values, and the long period distribution becomes narrower due to the increases number of lamellae in the stacks. With the further prolonged time of LLPS, the lamellae thicken, the averaged long period increases further, and the long period distribution becomes even more narrow. Therefore, we can conclude that the existence of

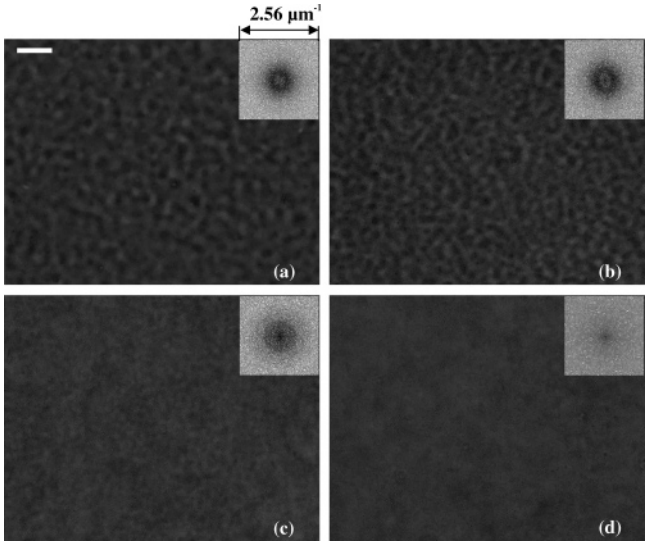

Figure 8. Phase contrast optical micrographs of H40 sample annealing at (a) 130, (b) 135, (c) 138, and (d) 140 °C for 6 h. The scale bar in (a) is 10 μm and is also applied to (b)−(d).

the minimum value of long period in Figure 5 is due to the competition between the amorphous PEB component inclusion and the PEH lamellar thickening. The balance between the above two mechanisms gives rise to the observed minimum long period with the LLPS time.

The quench depth and the LLPS time are two important factors to determine the concentration of the two phase-separated domains and the concentration fluctuation assisted nucleation rate which strongly affect the long period. Since the LLPS behavior is significantly controlled by the quench depth besides the LLPS time, we predicted that the minimum value of long period might also exist due to the quench depth of LLPS, and thus we further examined the influence of quench depth of LLPS on evolution of lamellar long period of the blend. Figure 8 shows the phase contrast optical micrographs of the H40 sample melted at 160 °C for 10 min and then isothermally annealed at 130, 135, 138, and 140 °C for 6 h. The 2D FFT images are shown as insets, which can indicate the diameters of the spinodal rings. The bicontinuous and interconnected tubelike structure characteristic of the late stages of spinodal decomposition can be clearly seen. The sizes of interconnected tubelike structure increase, indicating the increasing of the LLPS rate with the decreasing temperature. The bicontinuous structure cannot be clearly observed at 140 °C due to the very low LLPS rate. The above observation is easily understood from the decreasing thermodynamic driving force for LLPS with the increasing temperature.

Figure 9 shows atomic force micrographs of H40 sample isothermally crystallized at 117 °C for 64 min after annealing at 130, 135, 138, and 140 °C for 6 h. We have seen from Figure 8 that for the LLPS at temperature above 138 °C the bicontinuous structures become less obvious; for instance, the continuous PEB-rich domains cannot be even observed at 140 °C. At the high LLPS temperature, the rate of LLPS is slow due to the small thermodynamic driving force, while the difference in the coexistent compositions at 140 °C is ca. 0.26. The slow rate of LLPS and the closeness of the coexistent compositions together give rise to the relatively high PEB concentrations in the PEH-rich domains. Therefore, crystallization can occur in both the PEH-rich and PEB-rich domains because of the relatively high PEH concentrations in both domains compared with the case at the low LLPS temperature.

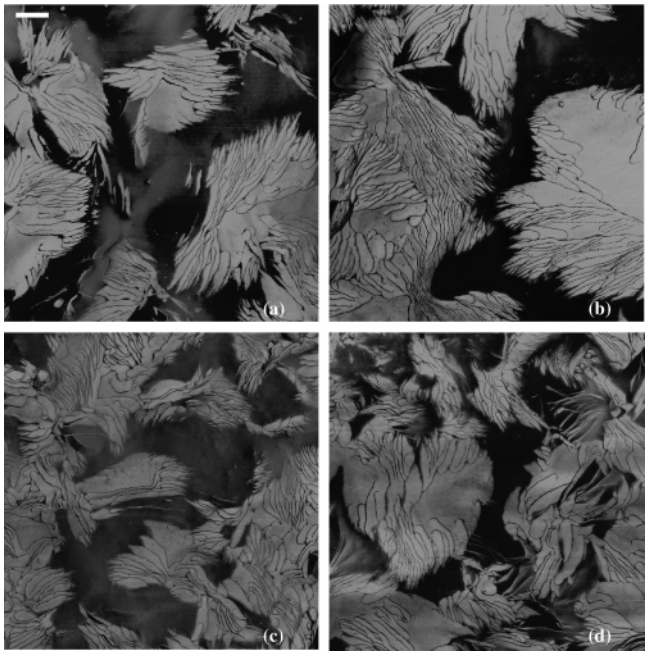

Figure 9. Atomic force micrographs of H40 sample isothermally crystallized at 117 °C for 64 min after annealing at (a) 130, (b) 135, (c) 138, and (d) 140 °C for 6 h. The scale bar in (a) corresponds to 1 μm and also applies to (b)−(d).

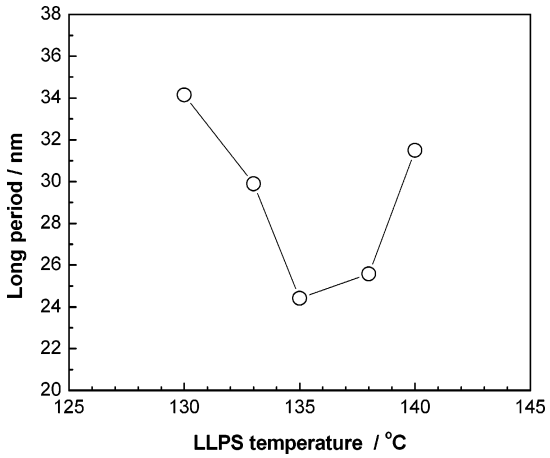

Figure 10. LLPS temperature dependence of the long period of H40 sample isothermally crystallized at 117 °C for 64 min.

A few small and short lamellae crystals in Figure 9c,d are, more or less, close to that shown in Figure 4a due to the weak LLPS at the high temperature. However, the influence of LLPS is still more distinct in Figure 9c,d than that in Figure 4a. It is noted that a few small and short lamellae can be observed in the PEB-rich domains in Figure 9c,d, indicating the less complete LLPS processes at these two temperatures of 138 and 140 °C. The amounts of the small and short lamellae are much less than that in Figure 4a. For the temperature below 138 °C, the bicontinuous structure can be clearly observed due to the relatively high rate of LLPS. The crystals are more clearly in the PEH-rich domains, and the crystals formed in the PEB-rich domains are basically absent (Figure 9a,b).

By analysis on the AFM height images in Figure 9, the averaged long periods can be obtained. Figure 10 shows the long periods of H40 sample isothermally crystallized at 117 °C for 64 min after LLPS at different temperatures for 6 h. As predicted, a similar trend to that shown in Figure 5 is found. The long period decreases at first and reaches the minimum value at about 135 °C and then increases with the increasing

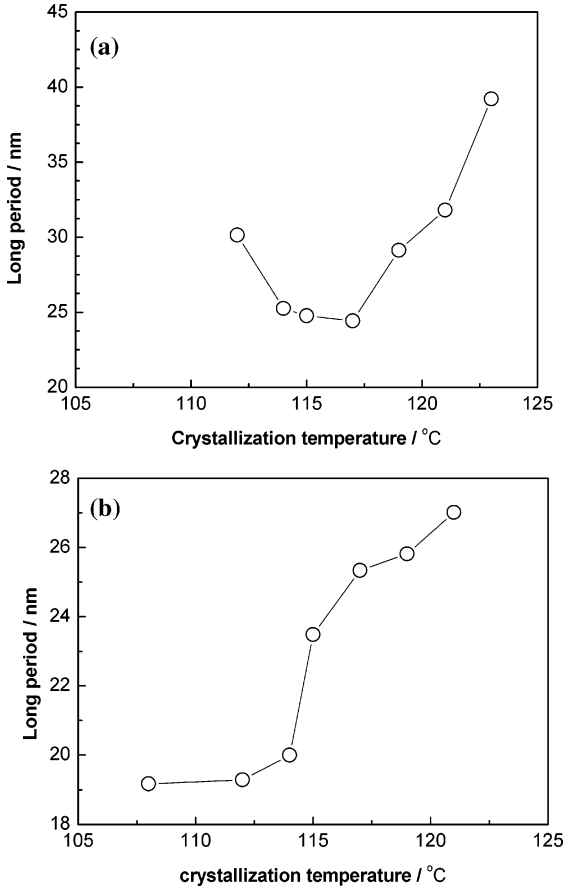

Figure 11. Changes of long periods of the samples isothermally crystallized at different temperatures for 64 min (a) H40 with LLPS at 135 °C for 6 h and (b) pure PEH.

temperature of LLPS. Our explanation for the above observed phenomenon can be as follows. At above 135 °C, the rate of LLPS decreases with the increasing LLPS temperature. The slow rate of LLPS and the closeness of the coexistent compositions give rise to the relatively high PEB concentrations in the PEH-rich domains. When the sample is quenched to the crystallization temperature, nucleation for crystallization can easily happen due to the assistance of spinodal LLPS.[19,20] The fast nucleation for crystallization due to the assistance of spinodal LLPS and the hindrance of noncrystallizable PEB component on the PEH crystal growth fronts can give rise to the amorphous component inclusion, which should be the major contribution to the increasing long period with the increasing temperature at above 135 °C. For the case at the temperature below 135 °C, the less hindrance of noncrystallizable PEB component on the PEH crystal growth fronts and the lower crystallization rate can give rise to the thicker lamellae and accordingly the larger long periods. The whole trend in Figure 10 is similar to the effect of LLPS time as we have discussed in the previous section. We note that for the case of 135 °C, due to the less hindrance of the noncrystallizable PEB component, the lamellar thickening might occur, but its effect was considered to be very minor compared with the lamellar insertion.

Finally, we should examine the effect of crystallization temperature on the lamellar crystal stacks and compare it with that of pure PEH sample. Figure 11a shows long periods of H40 sample isothermally crystallized at different temperatures for 64 min after LLPS at 135 °C for 6 h. The long period of H40 sample decreases at first and reaches the minimum value at about 117 °C and then increases with the increasing temperature of crystallization. Below 117 °C, the higher the

crystallization temperature, the slower the crystallization rate and the higher the chain segmental mobility. Therefore, the noncrystallizable PEB components become much easier to be excluded out of the lamellar stacks, causing the decrease of the long period. While at temperatures above 117 °C, the long period increases with the increasing temperature, which is more probably due to the lamellar thickening. This thickening has been reported in other polyolefins such as polyethylene, long-chain alkane, and homogeneous copolymers of ethylene and 1-octene.[21−23] Lamellar thickening is an inherent consequence of chain-folding crystallization of long chain molecules. Although the folding process provides the fastest mode of crystal growth for linear polymer, it usually leaves the system in a metastable state containing high surface energy. If the chain possesses sufficient mobility, lamellar thickening can take place, which lowers the total free energy. This should be the main reason that lamellar thickening and long period increasing can be observed at the high crystallization temperature. Figure 11b shows the long period of pure PEH isothermally crystallized at different temperatures for 64 min. The long period of pure PEH only increases at the high crystallization temperatures obviously through the lamellar thickening. It is not surprising that the crystallization temperature dependence of the long period in pure PEH sample does not show the minimum value as that of H40 sample, simply because of the absence of the PEB component inclusion/exclusion into the crystal lamellar stacks.

Conclusions

We have studied the effect of LLPS on the lamellar crystal morphology in a near-critical blend of PEH and PEB components by using optical microscopy and atomic force microscopy. The LLPS plays an important role on modification of the lamellar long period of the blend. The lamellar insertion and amorphous component exclusion models can be used to explain the decreasing long period, while the lamellar thickening and amorphous component inclusion models give rise to the increasing long period of the blend. The lamellar insertion and the lamellar thickening cause a narrow distribution of the local lamellar long periods. The competition and balance among the lamellar insertion, lamellar thickening, and the amorphous component inclusion/exclusion models give rise to the minimum long periods related to the LLPS temperature, LLPS time, and the crystallization temperature, respectively.

Acknowledgment. The authors acknowledge financial support of KJCX2-SW-H107, 2003CB615600, 20490220, and 10590355. Z. G. Wang thanks the financial support from "One Hundred Young Talents Program of Chinese Academy of Sciences".

References and Notes

(1) Crist, B.; Hill, M. J. *J. Polym. Sci., Polym. Phys.* **1997**, *35*, 2329.
(2) Mandelkern, L.; Alamo, R. G.; Wignall, G. D.; Stehlin, E. C. *Trends. Polym. Sci.* **1996**, *4*, 377.
(3) Hill, M. J.; Barham, P. J. *Polymer* **2000**, *41*, 1621.
(4) Wang, H.; Shimizu, K.; Hobbie, E. K.; Wang, Z. G.; Meredith, J. C.; Arim, A.; Amis, E. J.; Hsiao, B. S.; Hsieh, E. T.; Han, C. C. *Macromolecules* **2002**, *35*, 1072.
(5) Di Marzio, E. *Prog. Polym. Sci.* **1999**, *24*, 329.
(6) Wang, H.; Shimizu, K.; Kim, H.; Hobbie, E. K.; Wang, Z. G; Han, C. C. *J. Chem. Phys.* **2002**, *116*, 7311.
(7) Matsuba, G.; Shimizu, K.; Wang, H.; Wang, Z. G.; Han, C. C. *Polymer* **2004**, *45*, 5137.
(8) Wang, Z. G.; Wang, H.; Shimizu, K.; Dong, J. Y.; Hsiao, B. S.; Han, C. C. *Polymer* **2005**, *46*, 2675.
(9) Balsara, N. P.; Fetters, L. J.; Hadjichristidis, N.; Lohse, D. J.; Han, C. C.; Graessley, W. W.; Krishnamoorti, R. *Macromolecules* **1992**, *25*, 6137.
(10) Rhee, J.; Crist, B. *J. Chem. Phys.* **1993**, *98*, 4174.
(11) Briber, R.; Khoury, F. *Polymer* **1987**, *28*, 38.
(12) Briber, R.; Khoury, F. *J. Polym. Sci., Polym. Phys. Ed.* **1993**, *31*, 1253.
(13) Barham, P. J.; Hill, M. J.; Keller, A.; Rosney, C. C. A. *J. Mater. Sci., Lett.* **1998**, *7*, 1271.
(14) Hill, M. J.; Barham, P. J.; Keller, A.; Rosney, C. C. A. *Polymer* **1991**, *32*, 1384.
(15) Shimizu, K.; Wang, H.; Wang, Z. G.; Matsuba, G.; Kim, H.; Han, C. C. *Polymer* **2004**, *45*, 7061.
(16) Zhang, X. H.; Wang, Z. G.; Han, C. C. *Macromolecules* **2006**, *39*, 7441.
(17) Ivanov, D. A.; Amalou, Z.; Magonov, S. N. *Macromolecules* **2001**, *34*, 8944.
(18) Ivanov, D. A.; Legras, R.; Jonas, A. M. *Macromolecules* **1999**, *32*, 1582.
(19) Zhang, X. H.; Wang, Z. G.; Muthukumar, M.; Han, C. C. *Macromol. Rapid Commun.* **2005**, *26*, 1285.
(20) Zhang, X. H.; Wang, Z. G.; Dong, X.; Wang, D. J.; Han, C. C. *J. Chem. Phys.* **2006**, *125*, 024907.
(21) Rastogi, S.; Spoelstra, A. B.; Goossens, J. P. G.; Lemstra, P. J. *Macromolecules* **1997**, *30*, 7880.
(22) Winkel, A. K.; Hobbs, J. K.; Miles, M. J. *Polymer* **2000**, *41*, 8791.
(23) Goderis, B.; Peeters, M.; Mathot, V. B. F.; Koch, M. H. J.; Bras, W.; Ryan, A. J.; Reynaers, H. *J. Polym. Sci., Polym. Phys.* **2000**, *38*, 1975.

MA061801A